

Macroscopic Modelling and Simulation of Multi-Lane Traffic

Anargiros I. Delis
School of Production
Engineering & Management
Technical University of Crete
Chania, Crete, Greece 73100
Email: adelis@science.tuc.gr

Ioannis K. Nikolos
School of Production
Engineering & Management
Technical University of Crete
Chania, Crete, Greece 73100
Email: jnikolo@dpem.tuc.gr

Markos Papageorgiou
School of Production
Engineering & Management
Technical University of Crete
Chania, Crete, Greece 73100
Email: markos@dssl.tuc.gr

Abstract—In this work a macroscopic lane-changing model is incorporated to a single-class second-order gas-kinetic (GKT) traffic flow model to simulate multi-lane traffic flow dynamics. The lane-changing terms, simulating lane-changes due to vehicle interactions as well as spontaneous ones, are introduced as source and sink terms into the traffic flow equations. The numerical integration is based on an accurate and robust high-resolution finite volume relaxation scheme, where the nonlinear system of the macroscopic partial differential equations are first recast to a diagonalizable semi-linear system. A fifth order in space WENO scheme is used for spatial discretization, while time integration is based on a high-order implicit-explicit Runge-Kutta method. Numerical simulations, considering a two-lane highway flow where a bottleneck is formed due to a lane closure, demonstrate the ability of the proposed methodology to efficiently simulate the corresponding traffic dynamics.

I. INTRODUCTION

Macroscopic traffic flow modelling has been widely used, not only as a practical tool for efficiently simulating and optimizing traffic flow for specific infrastructures, but also as a research tool to analyze interesting phenomena, resulting from non-linear vehicle interactions, such as stop-and-go waves [10]. The existence of multiple lanes (with possible lane-drops, due to accidents or public works), on- and off-ramps, and intersections, necessitates the development of proper multi-lane models, which may effectively simulate vehicle lane-changes and overtaking maneuvers.

Relatively few works are available on the macroscopic modelling of the lane changing process, despite the recent advances in macroscopic modelling of traffic flow dynamics. In [8] a two dimensional with respect to space, first-order model is derived, along with a one-dimensional second-order dynamic one. In [3] a continuum model for two-lane traffic flow was proposed, based on the theory of kinematic waves, as an extension of the LWR first-order macroscopic model. Later on, in [6], [7] a microscopic multi-lane model was initially developed; then, based on this model, an Enskog-like kinetic model was derived, while a second-order macroscopic model was finally deduced from the kinetic one. In [10] a macroscopic second-order model of mixed multi-lane freeway traffic was presented, derived from a gas-kinetic approach. Three different types of lane-changing maneuvers were considered; those due to interactions between vehicles, corresponding to overtaking maneuvers or lane changes to avoid interactions

with slower vehicles in front, spontaneous maneuvers and, finally, mandatory lane changes due to lane merging, on- or off-ramps, accidents etc. Further, in [9] a second-order macroscopic model for interrupted traffic streams, based on a gas-kinetic approach was also developed, being a refinement of the work in [10]. The derived model is able to explicitly take into account the lane-changing process between a ramp lane and the adjacent lane of the main stream, as well as other similar cases, such as lane-drops.

This paper follows and extends the works of some of the preceding authors and our previous work in [1]. In [1] an integrated methodology was introduced for the numerical simulation of various second-order non-equilibrium macroscopic models, where the relaxation approximation, from [4], was used to transform the nonlinear macroscopic traffic flow differential equations into a diagonalizable semi-linear problem. The resulting relaxation system was discretized using low- and high-order spatial reconstructions, leading to a numerical approach characterized by simplicity, accuracy and robustness.

Here, the aforementioned computational framework is extended to deal with (single-class) multi-lane traffic, including the simulation of lane-drops due to different situations. The GKT model is used as a basis in this work, as it was found able to simulate the hysteretic phase transitions to congested states, connected with the existence of on-ramps, or other types of bottlenecks [11], [2], [12]. Additional lane-changing terms are introduced as source/sink terms into the traffic flow equations in order to take into account lane-changes due to vehicle interactions as well as spontaneous ones. Lane changes due to vehicle interactions are simulated using properly defined lane-changing probabilities and interaction frequencies, adapted from the works in [6] [7]. The spontaneous lane-changes are taken as proportional to vehicle densities, with the proportionality factors being the transition rates, defined in [10]. Special treatment is followed for the region upstream a lane drop, where the flow of the closed lane should be distributed to the adjacent lane(s). We note that both the GKT model as well as multi-lane dynamics has been deduced from kinetic formulations but their proposed combination and numerical approximation in a novel one.

II. THE GKT MODEL AND ITS MULTI-LANE EXTENSION

In what follows, we will denote as functions in space, x , and time, t , $\rho(x, t)$ the vehicle or traffic density (number of

vehicles per unit length), $u(x, t)$ the average speed and $q = \rho u$ the traffic flow rate (number of vehicles per unit time). We present first the single-class single-lane GKT model in conservation law form with source terms, given as

$$\partial_t \rho + \partial_x (\rho u) = r_{rmp}, \quad (1)$$

$$\partial_t (\rho u) + \partial_x (\rho u^2 + \theta \rho) = \rho \left(\frac{V_e^* - u}{\tau} \right) + h_{rmp}. \quad (2)$$

Following from [12], the source term r_{rmp} in the continuity equation (1) denotes the effective source density from on-ramps (or off-ramps) with merging (diverging) length l_{rmp} and inflow $q_{rmp} > 0$ from (or outflow $q_{rmp} < 0$ to) the ramp, and is given as

$$r_{rmp}(x, t) = \begin{cases} \frac{q_{rmp}(t)}{l_{rmp}} & \text{if } x \text{ is within merging zone,} \\ 0 & \text{elsewhere.} \end{cases} \quad (3)$$

Further, in the momentum equation (2), the term h_{rmp} describes changes of the macroscopic local speed by assuming that on-ramp vehicles merge to the main road at speed $u_{rmp} < u$ and, conversely, that drivers reduce their speed to u_{rmp} before leaving the main road. Hence, this term is given as

$$h_{rmp}(x, t) = \frac{q \cdot r_{rmp}}{\rho} + \frac{(u_{rmp} - u)|q_{rmp}|}{l_{rmp}}. \quad (4)$$

We note that, usually, one assumes $u_{rmp} \approx u$ [2].

In equation (2), $\theta = A(\rho)u^2$ is a pressure-like term, with $A(\rho)$ being a density-dependent variance factor given by the Fermi function as:

$$A(\rho) = A_0 + \delta A \left[1 + \tanh \left(\frac{\rho - \rho_{cr}}{\delta \rho} \right) \right] \quad (5)$$

in which ρ_{cr} is the critical density, which reflects the boundary between free flow and congested traffic, with A_0 and $A_0 + 2\delta A$ the variance pre-factors between the two states; while $\delta \rho$ denotes the width of the transition region. Typical range of values for the constants A_0 , δA and $\delta \rho$, along with the typical range of the other parameters for this model can be found, for example, in [11], [2], [9], [12], [1]. These parameters are meaningful, measurable, and have the correct order of magnitude for highway traffic while they can be adapted to city traffic as well [12].

The model also includes a traffic relaxation term aiming to keep flow in equilibrium, with $V_e^* \equiv V_e^*(\rho, u, \rho_a, u_a)$ being the, non-local and dynamic, equilibrium speed (maximum out-of-danger velocity meant to mimic drivers' behavior) with τ being a relaxation time. V_e^* depends not only on the local density ρ and mean speed u , but also on the non-local density ρ_a and mean speed u_a , and is defined as

$$V_e^* = u_{\max} \left[1 - \frac{\theta + \theta_a}{2A(\rho_{\max})} \left(\frac{\rho_a T}{1 - \rho_a / \rho_{\max}} \right)^2 B(\delta u) \right]. \quad (6)$$

According to (6), V_e^* is given by the maximum velocity u_{\max} , reduced by a term that reflects necessary deceleration maneuvers. Both ρ_a and u_a are computed at an anticipated location $x_a = x + \gamma(1/\rho_{\max} + T \cdot u)$ with T being the desired time-gap and γ a scale factor. Finally, B is a so-called

Boltzmann (interaction) factor, which, with $\delta u = \frac{u - u_a}{\sqrt{\theta + \theta_a}}$, is defined as

$$B(\delta u) = 2 \left[\delta u \frac{e^{-\delta u^2/2}}{\sqrt{2\pi}} + (1 + \delta u^2) \int_{-\infty}^{\delta u} \frac{e^{-y^2/2}}{\sqrt{2\pi}} dy \right].$$

This term contains the standard normal distribution and the Gaussian error function and describes the dependence of the braking interaction on the dimensionless velocity difference δu between the actual location x and the anticipation location x_a .

The crucial difference between the GKT model and other macroscopic traffic flow models is its non-local character. The non-local relaxation term in (6) has smoothing properties similar to those of a viscosity term, but its effect is forwardly directed and, therefore, more realistic. In contrast to other macroscopic models, the steady-state speed-density relation, $V^e(\rho)$, is not explicitly given, but results from the steady-state on homogeneous roads.

Model equations (1)-(2) can be written in vector form, supplied with initial conditions, as

$$\begin{aligned} \partial_t \mathbf{u} + \partial_x \mathbf{f}(\mathbf{u}) &= \mathbf{s}(\mathbf{u}), \\ \mathbf{u}(x, 0) &= \mathbf{u}_0(x), \end{aligned} \quad (7)$$

where the functions \mathbf{u} , $\mathbf{f}(\mathbf{u})$ and $\mathbf{s}(\mathbf{u}) \in \mathbb{R}^2$ with $\mathbf{u} = [\rho, q]^T$, $\mathbf{f}(\mathbf{u}) = [\rho u, \rho u^2 + \theta \rho]^T$ and $\mathbf{s}(\mathbf{u}) = [r_{rmp}, (\rho V_e^* - \rho u)/\tau + h_{rmp}]^T$. Systems in the form of (7) can be rewritten in quasi-linear form

$$\partial_t \mathbf{u} + \mathbf{J}(\mathbf{u}) \partial_x \mathbf{u} = \mathbf{s}(\mathbf{u}), \quad (8)$$

where $\mathbf{J}(\mathbf{u}) = \frac{\partial \mathbf{f}}{\partial \mathbf{u}}$ is the Jacobian matrix, given as

$$\mathbf{J}(\mathbf{u}) = \begin{bmatrix} 0 & 1 \\ \frac{\partial P}{\partial \rho} - u^2 & \frac{\partial P}{\partial q} + 2u \end{bmatrix}, \quad \text{with } P = \rho \theta(\rho, u). \quad (9)$$

The Jacobian matrix has two distinct and real (positive) eigenvalues, for all physically reasonable parameter sets, given as

$$\lambda_{1,2} = u + \frac{1}{2} \frac{\partial P}{\partial q} \pm \sqrt{\left(\frac{1}{2} \frac{\partial P}{\partial q} \right)^2 + \frac{q}{r} \frac{\partial P}{\partial q} + \frac{\partial P}{\partial \rho}}, \quad (10)$$

which denote that the model equations constitute a strictly hyperbolic set of partial differential equations.

For the multi-lane extension of the GKT model we consider a road with $l = 1, 2, \dots, N$ lanes. Then system (7) can be given for each lane l as

$$\begin{aligned} \partial_t \mathbf{u}_l + \partial_x \mathbf{f}(\mathbf{u}_l) &= \mathbf{s}(\mathbf{u}_l) + \mathbf{w}_l(\mathbf{u}_1, \dots, \mathbf{u}_N), \\ \mathbf{u}_l(x, 0) &= \mathbf{u}_{l0}(x), \end{aligned} \quad (11)$$

where now the extra source term $\mathbf{w}_l(\mathbf{u}_1, \dots, \mathbf{u}_N) \in \mathbb{R}^2$ accounts for the sources and sinks due to lane-changing, resulting in a weakly coupled system of $2N$ -equations. In [6] a macroscopic approach to multi-lane dynamics has been deduced, following from a kinetic formulation, by taking into account the behavior of driver-vehicle units regarding overtaking, deceleration/acceleration, and lane-changing maneuvers.

Following [6] the (generic) form of each component of the lane-changing terms are adapted here as

$$w_l^{1,2} = \left(\frac{1}{T_{l-1}^L} u_{l-1}^{1,2} - \frac{1}{T_l^R} u_l^{1,2} \right) (1 - \delta_{l1}) + \left(\frac{1}{T_{l+1}^R} u_{l+1}^{1,2} - \frac{1}{T_l^L} u_l^{1,2} \right) (1 - \delta_{lN}) \quad (12)$$

where the terms $1/T_l^L$ and $1/T_l^R$ are the *lane changing rates* from lane l to the left $l+1$ and right $l-1$ lane, respectively, and δ_{ij} the Kronecker delta. These rates are given as

$$\frac{1}{T_l^L} = P_L(\rho_{l+1})\nu(\rho_l) + S_l^L \quad (13)$$

$$\frac{1}{T_l^R} = P_R(\rho_{l-1})(1 - P_L(\rho_{l+1}))\nu(\rho_l) + S_l^R, \quad (14)$$

with $P_{R,L}(\rho)$ are lane-changing probabilities due to vehicle interactions and $\nu(\rho)$ are interaction frequencies due to breaking and acceleration. For simplicity we assume here that $P_R(\rho) = P_L(\rho)$ and in Fig. 1 we show a plot of these normalized probabilities along with a plot of the interaction frequency. Similar probability and frequency distributions have been also proposed in [5], [7].

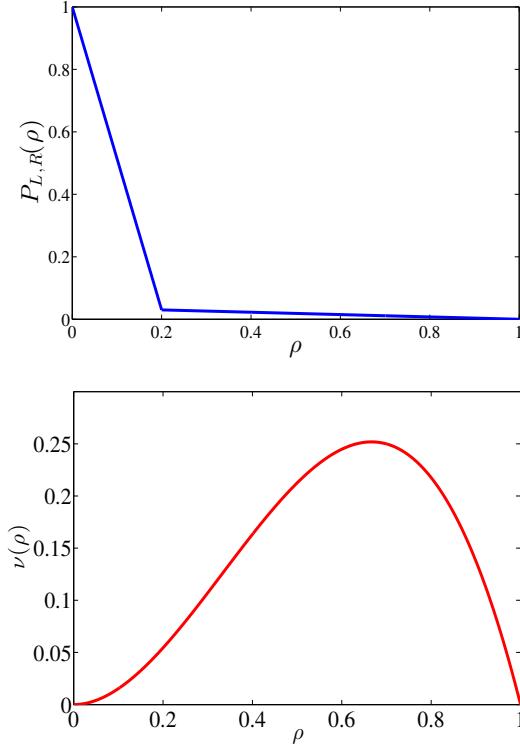


Fig. 1. Lane changing probability and frequency for normalized densities

Further in (13) and (14) we take into account spontaneous lane changes, which are not caused by interactions with other vehicles, through the terms $S_l^{R,L}$. This is particularly important for inhomogeneous traffic situations since both interactive and spontaneous lane changes are necessary for the description of empirically observable density-dependence of the total lane changing rates and lane occupancies. Following from [10], [9]

we assume that these terms depend on the density, ρ , and are given as

$$S_l^{R,L} = k_l^{R,L} \left(1 - \frac{\rho_{l\pm 1}}{\rho_{\max, l\pm 1}} \right)^\beta \quad (15)$$

where $k_l^{R,L}, \beta$ are spontaneous lane-changing factors.

III. THE RELAXATION APPROACH AND ITS NUMERICAL DISCRETIZATION

In this section we briefly present the class of relaxation models of [4] applied to various second-order macroscopic traffic flow models in [1]. Dropping, for simplicity, the lane index and by the introduction of the artificial, relaxation, variables \mathbf{v} , the corresponding to (11) relaxation system (with $\mathbf{r}(\mathbf{u}) = \mathbf{s}(\mathbf{u}) + \mathbf{w}(\mathbf{u})$) reads as

$$\begin{aligned} \partial_t \mathbf{u} + \partial_x \mathbf{v} &= \mathbf{r}(\mathbf{u}), \\ \partial_t \mathbf{v} + \mathbf{C}^2 \partial_x \mathbf{u} &= \frac{\mathbf{f}(\mathbf{u}) - \mathbf{v}}{\epsilon}, \end{aligned} \quad (16)$$

with initial data

$$\begin{aligned} \mathbf{u}(x, 0) &= \mathbf{u}_0(x), \\ \mathbf{v}(x, 0) &= \mathbf{v}_0(x) = \mathbf{f}(\mathbf{u}_0(x)), \end{aligned}$$

where the small parameter ϵ ($0 < \epsilon \ll 1$), is the *relaxation rate* and $\mathbf{C}^2 = \text{diag}\{c_1^2, c_2^2\}$ is a positive diagonal. Applying the Chapman-Enskog expansion in system (16), the following approximation for \mathbf{u} can be obtained,

$$\begin{aligned} \partial_t \mathbf{u} + \partial_x \mathbf{f}(\mathbf{u}) &= \mathbf{r}(\mathbf{u}) + \epsilon \partial_x \left[\left(\frac{\partial \mathbf{f}(\mathbf{u})}{\partial \mathbf{u}} \right) \mathbf{r}(\mathbf{u}) \right] + \\ &+ \epsilon \partial_x \left[\left(\mathbf{C}^2 - \left(\frac{\partial \mathbf{f}(\mathbf{u})}{\partial \mathbf{u}} \right)^2 \right) \partial_x \mathbf{u} \right] + O(\epsilon^2). \end{aligned} \quad (17)$$

Equation (17) controls the first-order behavior of system (16), with the third term on the right-hand side being an $O(\epsilon)$ dominant dissipation term in the model with $\left(\mathbf{C}^2 - \left(\frac{\partial \mathbf{f}(\mathbf{u})}{\partial \mathbf{u}} \right)^2 \right)$ being the diffusion-like coefficient matrix. Model (16) is well-posed only if this matrix is positive semi-definite for all \mathbf{u} . This requirement on the diffusion coefficient matrix is the well-known *sub-characteristic condition* [4], i.e.

$$\mathbf{C}^2 - \left(\frac{\partial \mathbf{f}(\mathbf{u})}{\partial \mathbf{u}} \right)^2 \geq 0, \quad \forall \mathbf{u}, \quad (18)$$

which ensures the dissipative nature of (17); and it is equivalent to

$$\lambda^2 \leq c^2, \quad \text{where } \lambda = \max_{1 \leq i \leq 2} |\lambda_i| \quad \text{and} \quad c = \min_{1 \leq i \leq 2} |c_i|. \quad (19)$$

Condition (18) can always be satisfied by choosing sufficiently large values for the diagonal elements in \mathbf{C}^2 , for \mathbf{u} varying in a bounded domain. As such, the solution of the relaxation model (16) converges strongly to the unique entropy solution of the original conservation laws.

System (16) can be easily diagonalized leading to the following decoupled system of equations:

$$\partial_t (\mathbf{v} + \mathbf{C}\mathbf{u}) + \mathbf{C} \partial_x (\mathbf{v} + \mathbf{C}\mathbf{u}) = \frac{\mathbf{f}(\mathbf{u}) - \mathbf{v}}{\epsilon} + \mathbf{C}\mathbf{r}(\mathbf{u}); \quad (20)$$

$$\partial_t (\mathbf{v} - \mathbf{C}\mathbf{u}) - \mathbf{C} \partial_x (\mathbf{v} - \mathbf{C}\mathbf{u}) = \frac{\mathbf{f}(\mathbf{u}) - \mathbf{v}}{\epsilon} - \mathbf{C}\mathbf{r}(\mathbf{u}). \quad (21)$$

The left-hand side of system (20)-(21) is linear with constant wave speeds, split into positive and negative parts. Thus, its solution has the property that it propagates at finite speeds along linear characteristic curves $dx/dt = \pm \mathbf{C}$. From (20)-(21) and by setting $\mathbf{g}_{1,2} = \mathbf{v} \pm \mathbf{C}\mathbf{u}$, the follow relations can be obtained that recover the original variables of the relaxation system,

$$\mathbf{u} = \frac{1}{2} \mathbf{C}^{-1} (\mathbf{g}_1 - \mathbf{g}_2) \quad \text{and} \quad \mathbf{v} = \frac{1}{2} (\mathbf{g}_1 + \mathbf{g}_2). \quad (22)$$

The structure of the linear characteristic field of the relaxation system constitutes a clear advantage compared to the original conservation laws for their numerical integration.

For the spatial discretization of (16) the finite volume approach is adopted. Let $x_i = i\Delta x$, $x_{i\pm\frac{1}{2}} = (i \pm \frac{1}{2})\Delta x$, where Δx is a uniform spatial discretization step. The discrete cell average of \mathbf{u} in the cell $I_i = [x_{i-\frac{1}{2}}, x_{i+\frac{1}{2}}]$ at time t is defined as $\mathbf{u}_i(t)$ and the approximate value of \mathbf{u} at $(x_{i+\frac{1}{2}}, t)$ by $\mathbf{u}_{i+\frac{1}{2}}(t)$. The semi-discrete relaxation system is given as

$$\begin{aligned} \frac{\partial}{\partial t} \mathbf{u}_i + \frac{1}{\Delta x} (\mathbf{v}_{i+\frac{1}{2}} - \mathbf{v}_{i-\frac{1}{2}}) &= \mathbf{r}(\mathbf{u})_i, \\ \frac{\partial}{\partial t} \mathbf{v}_i + \frac{\mathbf{C}^2}{\Delta x} (\mathbf{u}_{i+\frac{1}{2}} - \mathbf{u}_{i-\frac{1}{2}}) &= -\frac{1}{\epsilon} (\mathbf{v}_i - \mathbf{f}(\mathbf{u})_i). \end{aligned} \quad (23)$$

where $\mathbf{r}(\mathbf{u})_i$ and $\mathbf{f}(\mathbf{u})_i$ are discrete averages of the source term and flux function, respectively. To completely define the spatial discretization, we need to compute the flux values $\mathbf{u}_{i\pm\frac{1}{2}}$ and $\mathbf{v}_{i\pm\frac{1}{2}}$. As system (16) has linear characteristics and its characteristic speeds, $+c_k$ and $-c_k$, are constant, the construction of an upwind scheme is much simpler than developing such a scheme for the original nonlinear conservation laws. For example, the *first-order upwind* scheme, [4], [1], applied to \mathbf{g}_1 and \mathbf{g}_2 gives $\mathbf{g}_{1_{i+\frac{1}{2}}} = \mathbf{g}_{1_i}$ and $\mathbf{g}_{2_{i+\frac{1}{2}}} = \mathbf{g}_{2_{i+1}}$.

To increase the spatial order of accuracy, a WENO-type interpolant approach is applied, where the approximate solution is reconstructed using higher-order polynomials. By direct application of this reconstruction to the k -th components of the characteristic variables, $\mathbf{g}_{1,2} = \mathbf{v} \pm \mathbf{C}\mathbf{u}$, a non-oscillatory higher-order spatial discretization is obtained. The superiority of applying higher-order schemes, compared to low-order ones, in traffic flow simulations has been recently demonstrated in [1]. By applying a fifth-order WENO reconstruction the discrete values of each component of $\mathbf{g}_{1_{i+\frac{1}{2}}}$ and $\mathbf{g}_{2_{i+\frac{1}{2}}}$, at a cell boundary $i+\frac{1}{2}$, are defined as left and right extrapolated values $\mathbf{g}_{1_{i+\frac{1}{2}}}^-$ and $\mathbf{g}_{2_{i+\frac{1}{2}}}^+$ i.e., $\mathbf{g}_{1_{i+\frac{1}{2}}} = \mathbf{g}_{1_{i+\frac{1}{2}}}^-$ and $\mathbf{g}_{2_{i+\frac{1}{2}}} = \mathbf{g}_{2_{i+\frac{1}{2}}}^+$. After the reconstructions have been performed to each component of the characteristic variables, the numerical fluxes for $\mathbf{u}_{i+\frac{1}{2}}$ and $\mathbf{v}_{i+\frac{1}{2}}$ are computed from (22). In a similar manner we compute the face values at cell boundary $i - \frac{1}{2}$.

The semi-discrete relaxation system (23) constitutes a system of autonomous ordinary differential equations with a stiff relaxation term. A time marching approach based on implicit-explicit (IMEX) Runge-Kutta (RK) splitting was considered as to avoid the time step restrictions imposed by an explicit solver due to stiffness. As such, the explicit RK scheme treats the non-stiff stage of the splitting while a diagonally implicit RK scheme treats the stiff one. We note that even though an implicit scheme is used, either linear or nonlinear algebraic

equations have to be solved due to the special structure of the relaxation system. The choice of the time marching step Δt^n is based only on a usual CFL condition,

$$CFL = \max \left(\left(\max_{i,k} c_k^n \right) \frac{\Delta t^n}{\Delta x}, \frac{\Delta t^n}{\Delta x} \right) \leq \frac{1}{2},$$

where the values of the relaxation constants c_k^n are re-computed at each time step based on the Jacobian eigenvalues as to satisfy the sub-characteristic condition (18). For a detailed presentation of the spatial and temporal discretizations, as well as the treatment of boundary conditions and source term computations, we refer to [1].

IV. SIMULATIONS AND RESULTS

We present single-class simulations of the interesting case of a two-lane ($N = 2$) bottleneck, corresponding to a lane closure or an accident. We assume that the right lane closes at a certain point x_e . To model the behavior close to the bottleneck, we specify a mandatory lane changing for the right to left, since all drivers there must merge into the adjacent lane. To achieve a smooth transition we assume a merging length $l_m = 500$ m in front of the lane closure which acts in the same way as l_{tmp} in equations (3)-(4). To guarantee that all vehicles have changed lane at x_e we assume that this mandatory lane-changing, as given in equations (1)-(4), grows inversely to the distance $L = x_e - x$ and we achieve this by multiplying the effective densities and flows with a smooth step-like function $m(x)$, similar to (5), with $m(x_e - l_m) \approx 0$ and $m(x_e) \approx 1$. Further, and within the merging length, the V_e^* values for the right lane are substituted with the left lane velocities as to realistically describe the drivers' behavior of adapting their velocity to that of the lane to which they merge.

For the spontaneous lane-changing terms (15) we adopt the European-rule of primarily using the right lane at low densities [10]. Calibration results have shown that spontaneous lane-changing influences mainly low-density regimes. Setting $\beta = 8$ in (15), a smooth correction pre-factor G_{Eu} , with $0 < G_{Eu}(\rho) < 1$, is used to account for the European traffic rule by modifying S_1^L as $S_1^L G_{Eu}$ and S_2^R as S_2^R / G_{Eu} . The G_{Eu} function used and the final forms of S_1^L and S_2^R are shown in Fig. 2.

The model parameters used in the simulations are given in Table I and follow close the ones given in [10], [9] and have been calibrated to traffic data from the Dutch motorway A9. In the numerical discretization $\Delta x = 20m$, the CFL value was set to 0.25 and the relaxation rate in (16) $\epsilon = 10^{-8}$.

TABLE I. PARAMETERS USED FOR THE TWO-LANE GKT TRAFFIC MODEL

| Model parameters | Units | Right lane | Left lane |
|------------------|--------|--------------------|--------------------|
| u_{\max} | km/h | 90 | 110 |
| ρ_{\max} | veh/km | 150 | 150 |
| ρ_{cr} | veh/km | $0.275\rho_{\max}$ | $0.036\rho_{\max}$ |
| T | s | 1.7 | 1.2 |
| γ | | 1.2 | 1.2 |
| τ | s | 35 | 35 |
| A_0 | | 0.007 | 0.0065 |
| δA | | 0.015 | 0.018 |
| $\delta\rho$ | veh/km | $0.055\rho_{\max}$ | $0.05\rho_{\max}$ |
| $k_l^{R,L}$ | | 75 | 28 |

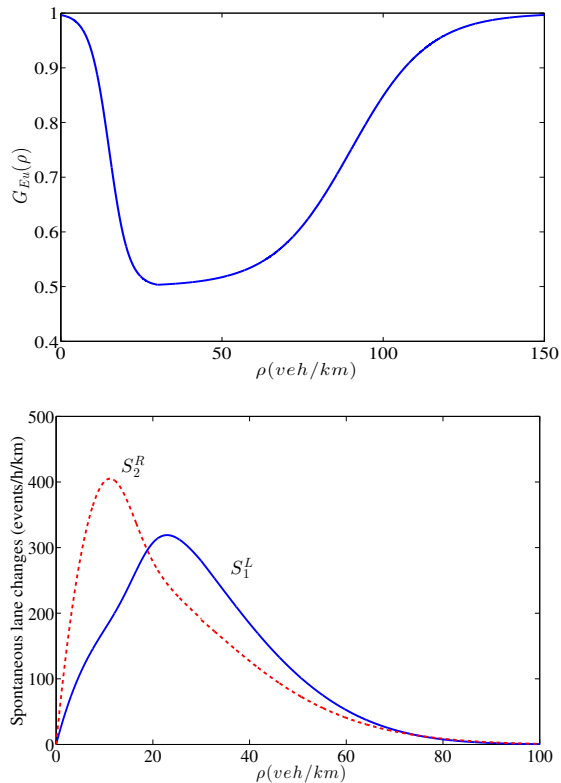


Fig. 2. The pre-factor G_{Eu} (top) and the modified spontaneous lane changing rates

We start with an empty 10 km two-lane highway with a closure at $x_e = 5$ km on the right lane and prescribe the incoming values at the boundary $x = 0$. The prescribed density is the same for both lanes and the prescribed flow is assumed to be in equilibrium. The traffic dynamics are essentially characterized by the approaching traffic volume. The first simulation is for a low incoming density $\rho_0 = 12.5$ veh/km and the density spatio-temporal evolution can be seen in Fig. 3 for a total time of 20 min. Starting with an empty highway one observes the free flow of the vehicles until the stretch is completely filled. For this case the capacity of the left lane is sufficient enough to accommodate the vehicle flow from both lanes, resulting in a higher density (but free flow) in the left lane downstream of the bottleneck, whereas the right lane is empty behind the closure.

The second simulation is for $\rho_0 = 25$ veh/km. The vehicle density spatio-temporal evolution can be seen in Fig. 4. After free flow and when the stretch is completely filled, the density rises at the bottleneck. A growing region of congested traffic forms, since the capacity of the left lane is exceeded by the traffic volume in both lanes. Later one observes the formation of a traffic jam, which is finally moving backwards on both lanes, while homogeneous free flow can be observed downstream of the bottleneck in the left lane. As it was noted also in [10], the observed step-like structure of the congested region, of both lanes, is related to deceleration in two steps, i.e. rough breaking and fine breaking, when approaching the traffic jam from free flow. The density and flow per lane are shown in Fig. 5. These results are, at least qualitatively, similar to those observed in real traffic flow situations and agree to

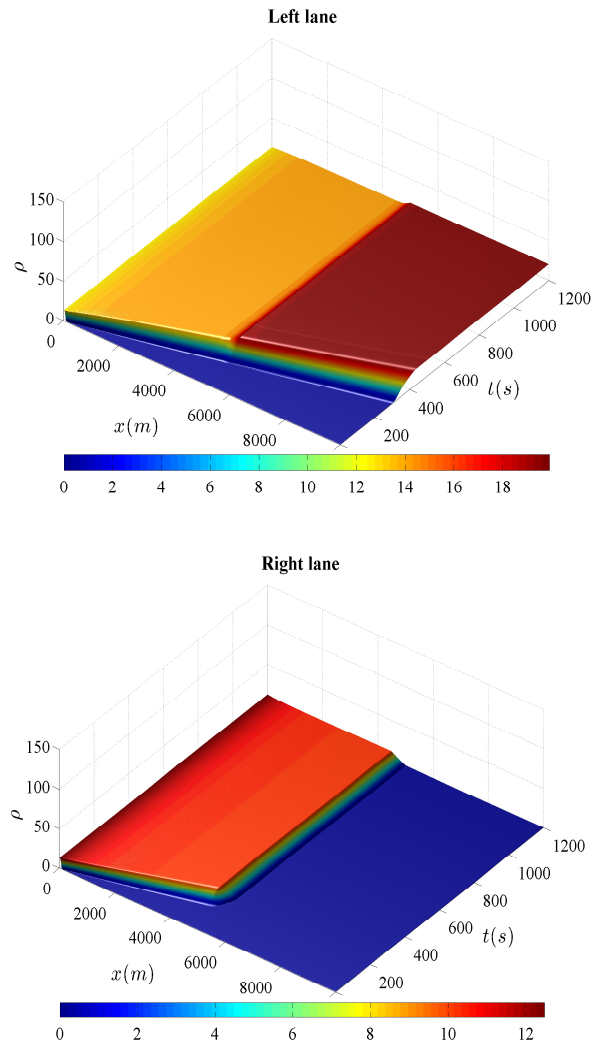


Fig. 3. Spatio-temporal evolution for density in each lane $\rho_0 = 12.5$ veh/km

similar simulations tests from [10], [2] and [7].

V. CONCLUSIONS

A novel way of extending a macroscopic second-order traffic flow model for the simulation of multi-lane traffic dynamics has been presented. The second-order non-equilibrium GKT traffic model was used as the basis model since, due to its non-local character, it allows to describe the fluctuations of speed dynamics around a so-called equilibrium speed-density relationship. The GKT model as well as multi-lane dynamics have been deduced from kinetic formulations. Both interactive and spontaneous lane changes are explicitly taken into account by the proposed model which aim to describe the behavior of driver-vehicle units regarding overtaking, deceleration/acceleration, and lane-changing maneuvers. An important part of the simulation process is the stable and accurate numerical solution of the resulting model by the development of a high-resolution finite volume relaxation scheme. Numerical simulations for a two-lane highway with a lane closure have demonstrated the ability of the proposed model to describe traffic dynamics at bottlenecks, producing results similar to those observed in real traffic flow situations

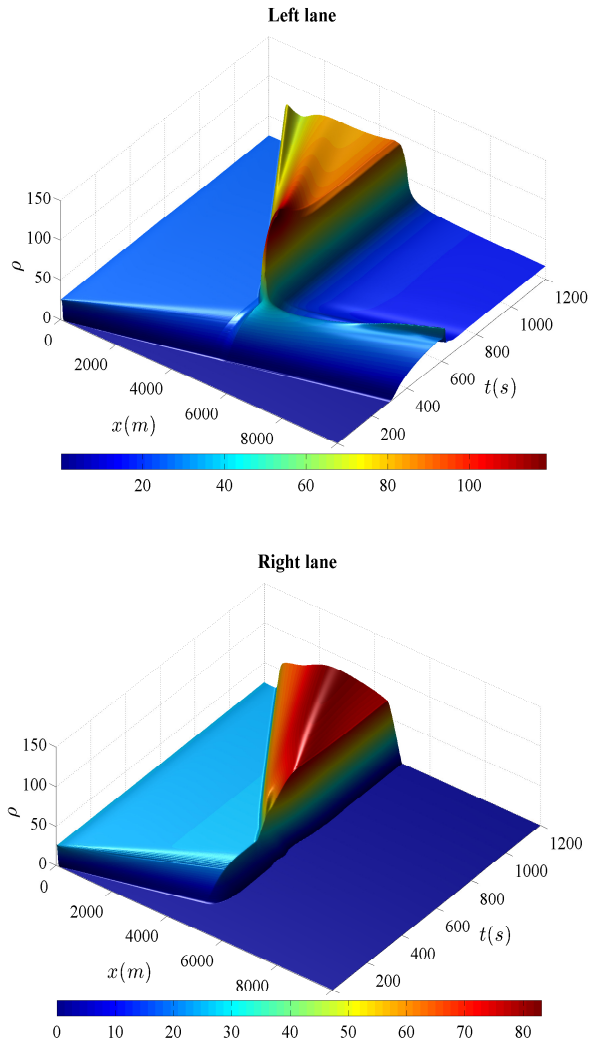


Fig. 4. Spatio-temporal evolution for density in each lane for $\rho_0 = 25$ veh/km

and to similar simulation results from the literature. Following from this presentation, our ongoing work focuses on the multi-class extension and calibration of the model as to realistically describe the effects of heterogeneous traffic.

ACKNOWLEDGMENT

This research was supported by TRAMAN21 ERC Advanced Investigator Grand under the European Union's Seventh Framework Programme (FP/2007-20013).

REFERENCES

- [1] A.I. Delis, I.K. Nikolos and M. Papageorgiou, High-resolution numerical relaxation approximations to second-order macroscopic traffic flow models, *Transportation Research Part C: Emerging Technologies*, vol 44, pp. 318-349, 2014.
- [2] D. Helbing, A. Hennecke, V. Shvetsov and M. Treiber, MASTER: Macroscopic traffic simulation based on a gas-kinetic, non-local traffic model, *Transportation Research Part B: Methodological*, vol 35, pp. 183-211, 2001.
- [3] E.N. Holland and A.W. Woods, A continuum model for the dispersion of traffic on two-lane roads, *Transportation Research Part B: Methodological*, vol 31, pp. 473-485, 1997.

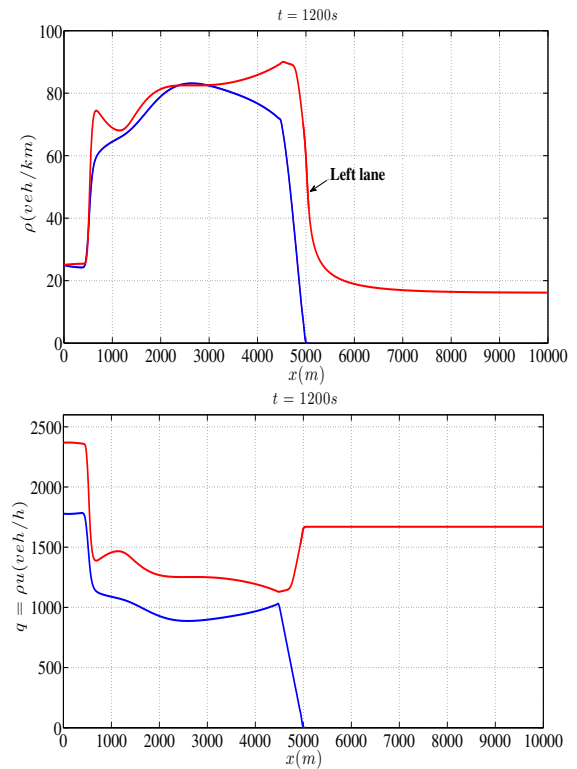


Fig. 5. Density (top) and flow (bottom) for the two lanes at time $t = 1200$ s for $\rho_0 = 25$ veh/km

- [4] S. Jin S. and Z. Xin Z., The relaxing schemes of conservation laws in arbitrary space dimensions, *Comm. Pure Appl. Math.*, vol. 48, pp. 235-277, 1995.
- [5] A. Klar and R. Wegener, Enskog-like kinetic models for vehicular traffic *Journal of statistical Physics*, vol. 87, pp.91-114, 1997.
- [6] A. Klar and R. Wegener, Hierarchy of models for multilane vehicular traffic I: Modeling, *SIAM Journal on Applied Mathematics*, vol. 59, pp.983-1001, 1998.
- [7] A. Klar and R. Wegener, Hierarchy of models for multilane vehicular traffic II: Numerical Investigations, *SIAM Journal on Applied Mathematics*, vol. 59, pp. 1002-1011, 1998.
- [8] P.G. Michalopoulos, D.E. Beskos and Y. Yamauchi, Multilane traffic flow dynamics: Some macroscopic considerations, *Transportation Research Part B: Methodological*, vol. 18, pp.377-395, 1984.
- [9] D. Ngoduy, *Macroscopic discontinuity modeling for multiclass multilane traffic flow operations*, Ph.D. Thesis, Delft University of Technology, 2006.
- [10] V. Shvetsov and D. Helbing, Macroscopic dynamics of multi-lane traffic, *Physical Review E - Statistical Physics, Plasmas, Fluids, and Related Interdisciplinary Topics*, vol 56, pp. 6328-6339, 1999.
- [11] M. Treiber, A. Hennecke and D. Helbing, Derivation, properties, and simulation of a gas-kinetic-based, nonlocal traffic model, *Physical Review E - Statistical Physics, Plasmas, Fluids, and Related Interdisciplinary Topics*, vol 59, pp. 239-253, 1999.
- [12] M. Treiber and A. Kesting, *Traffic flow dynamics: Data, models and simulation*, Springer, 2013.